Vol. 53: 25–41, 2012
doi: 10.3354/cr01081

CLIMATE RESEARCH
Clim Res

Published online May 8

Annual regional precipitation variations from a 700 year tree-ring record in south Tibet, western China

Jingjing Liu[1], Bao Yang[1,2,*], Kai Huang[1], Dmitry M. Sonechkin[3]

[1]Key Laboratory of Desert and Desertification, Cold and Arid Regions Environmental and Engineering Research Institute, Chinese Academy of Sciences, 730000 Lanzhou, PR China

[2]MOE Key Laboratory of West China's Environmental System College of Earth and Environment Sciences, Lanzhou University, 730000 Lanzhou, PR China

[3]P. P. Shirshov Oceanology Institute, Russian Academy of Sciences, Nakhimowskii Prospect 36, Moscow 117997, Russia

ABSTRACT: Newly measured tree-ring series from 114 living and dead cypress *Cupressus gigantea* were collected from 2 high-elevation sites in the Langxian region in south Tibet, western China. Combined with 2 previous ring-width data sets from southern Tibet, the composite chronology correlated at 0.563 with instrumental precipitation over the 1961–2009 period. The low-frequency component of the chronology shows a higher correlation of 0.77 with instrumental data. We reconstructed the annual precipitation (July–June) from A.D. 1300 to 2010 for southern Tibet based on the scaling method. Wet conditions occurred in 1342–1391, 1383–1387, 1408–1423, 1453–1458, 1473–1492, 1508–1524, 1657–1667, 1701–1731, 1742–1768, 1781–1788, 1854–1868, 1917–1933, and 1994–2006, whereas dry years prevailed during 1388–1407, 1424–1452, 1459–1472, 1493–1507, 1525–1656, 1668–1700, 1732–1741, 1769–1780, 1789–1853, 1869–1916, and 1934–1993. Spatial correlation revealed that the annual precipitation reconstruction contained a strong regional precipitation signal for the southern Tibetan Plateau (TP). Coherent moisture variations on the southern TP over the past 700 yr were identified by comparison with other tree-ring-based drought reconstructions of the nearby regions. The reconstructed series showed that high (low) precipitation periods on the southern TP corresponded with dry (wet) spells on the northern TP during most of the past 500 yr, suggesting the influence of different moisture sources from the Westerlies and the south Asian summer monsoon on the northern and southern TP, respectively. The possible mechanism was related to the shift of the convergence shear line and a teleconnection of the North Atlantic Oscillation (NAO) through controlling moisture via the Westerlies.

KEY WORDS: Tree ring · Climate change · Tibetan Plateau · Westerlies · South Asian summer monsoon · North Atlantic Oscillation

1. INTRODUCTION

The Tibetan Plateau (TP) plays a key role in climate change in China (Shi et al. 1999), owing to its extreme topography and its location in subtropical latitudes. It creates an important climatic force as a result of its influence on the large-scale atmospheric circulation in Asian monsoons (Webster et al. 1998). To understand spatial and temporal climate variations over the TP, it is thus vital to improve our knowledge of Asian monsoon dynamics. However, relatively short instrumental records (spanning only the last 50 yr or so) and the scarcity of meteorological stations hinder access to long-term (decadal to centennial) climatic variations on the TP. As tree rings can provide annually resolved and precisely dated

*Corresponding author. Email: yangbao@lzb.ac.cn

climate information, they have been widely used for climate reconstructions. Previous studies on tree rings on the TP have been carried out in the northeastern (Sheppard et al. 2004, Tian et al. 2007, 2009, Gou et al. 2008, Zhang et al. 2009, 2010, Qin et al. 2010, Liu et al. 2010a, Shao et al. 2010, Yang et al. 2010a, 2011) and southeastern regions (Bräuning 2001, Liang et al. 2008, Yang et al. 2010b,c, Li et al. 2011). Nevertheless, regional climatic variations over the past centuries on the TP are still not well understood.

Here we developed a new millennium-long tree-ring chronology at the Langxian region in the interior part of the southern TP. We worked on a regional perspective, combining the new Langxian samples with 2 previous tree-ring data sets from the Sangri and Langkazi regions (Liu et al. 2010b, 2011) in central Tibet to form a new composite chronology. We compared our climatic reconstruction with the monsoonal Asian Palmer drought severity index (PDSI) reconstruction from Cook et al. (2010) and other tree-ring reconstructions in nearby areas to reveal regional climatic variations over the past 700 yr and their possible dynamics.

2. MATERIALS AND METHODS

2.1. Geographical setting

Our study region (28.90 to 29.00° N, 93.30 to 93.33° E; 3080 to 3420 m above sea level [m.a.s.l.]) (Fig. 1) is located on the banks of the middle reaches of the Yarlung Tsangpo River Valley in southern Tibet. The terrain gradually ascends from both banks of the river. The average elevation of this area is 3200 m a.s.l., with >60% of the land area reaching 3500 m. The region is influenced by the rain shadow of the moun-

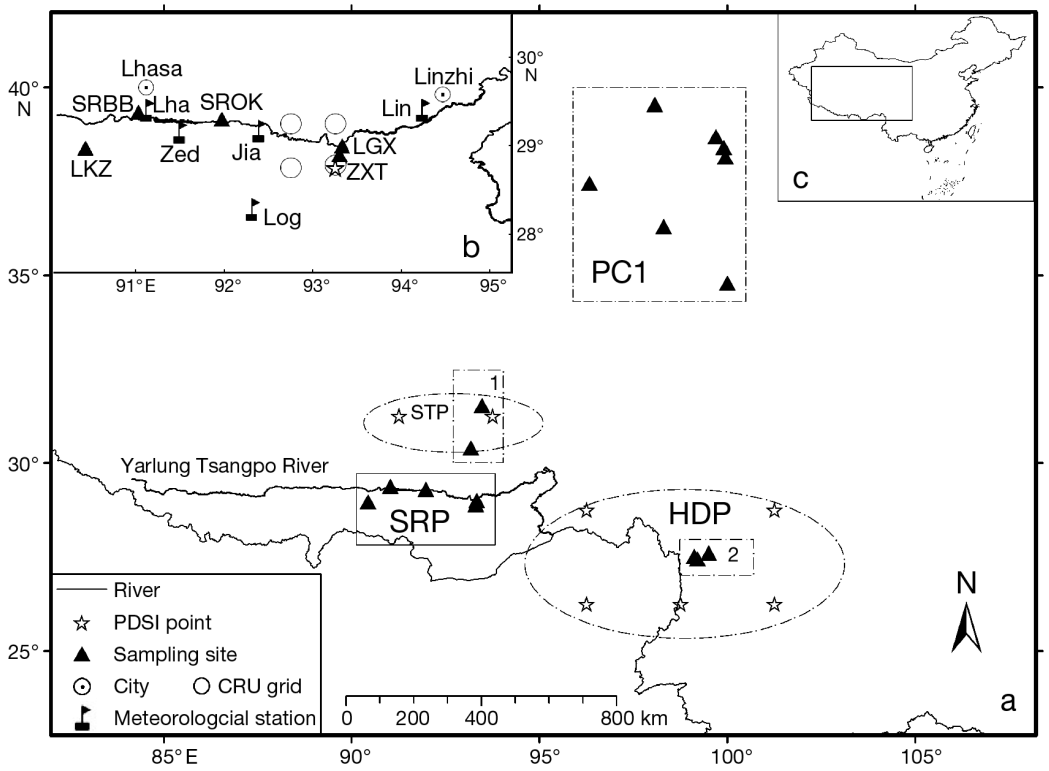

Fig. 1. (a) Locations of moisture-sensitive reconstructions on the Tibetan Plateau (TP). PC1: 7 tree-ring sampling sites on the northern TP (Yang et al. 2010a); HDP: 5 gridded Palmer severity drought index (PDSI) reconstructions in the Hengduan Mountains, southeastern TP (Cook et al. 2010); STP: 2 gridded PDSI reconstructions, southern TP (Cook et al. 2010); SRP: 5 tree-ring sampling sites on the southern TP (present study; see b); Rectangle 1: 2 tree-ring sampling sites in northern Tibet (Wang et al. 2008); Rectangle 2: 3 tree-ring sampling sites in the Hengduan Mountains (Fang et al. 2010). Black triangles: tree-ring sites; stars: PDSI grids. (b) Locations of sampling sites and instrumental data for the present study. LKZ is the tree-ring site in Langkazi County (Liu et al. 2010b); SRBB and SRQK are the tree-ring sites in Sangri County (Liu et al. 2011); and ZXT and LGX are the tree-ring sites in Langxian County (present study). Lin, Jia, Log, Lha, and Zed are abbreviations for Linzhi, Jiacha, Longzi, Lhasa, and Zedang stations, respectively. White dots: 4-gridded monthly precipitation data of CRUts2.1 from Mitchell and Jones (2005) (0.5° × 0.5°; the original data can be downloaded from www.cru.uea.ac.uk/cru/data/hrg/); star: the closest PDSI grid (Dai et al. 2004). (c) Location within China

tains and enjoys a temperate and semi-humid climate; the majority of rainfall occurs from May to September. The mean annual temperature is 11.2°C and the average annual sunshine is between 2000 and 2500 h. Pines *Pinus densata*, larch *Larix* spp., firs *Abies* spp., junipers *Sabina tibetica*, and cypress *Cupressus gigantea* constitute the main forestry in the region, with a landscape of exuberant grass and bush stands in the alpine shrubby steppe soil.

The study region is situated in the interior TP, which is greatly influenced by 2 large-scale atmospheric circulation systems, the south Asian summer monsoon (SASM) and the Westerlies. The SASM is one of the most important Asian monsoon systems (Huang et al. 1998), affecting continental Asia from mid May to late September. Tropical ocean areas, especially in the Arabian Sea, the Bay of Bengal, and the Indian Ocean, provide sufficient energy and vapor for the SASM to provide ample precipitation to continental Asia (Mohanty et al. 1996). The Westerlies dominate the atmospheric circulation pattern on the TP prior to the SASM and bring moisture from the ocean surface toward the TP. The moisture originating from the Westerlies in the non-monsoon season is vital for the interior TP, and its advance and retreat greatly affect the wet/dry variations (Tian et al. 2005).

2.2. Sampling

Cypress *Cupressus gigantea* is a non-shade-tolerant species standing on the adret slopes between 3000 and 3400 m a.s.l. in the mountain area of Langxian County. Two cypress sites were chosen in open forests 500 m from the Yarlung Tsangpo River. The ZXT site (28.90° N, 93.30° E; 3080 to 3420 m a.s.l.) is located on the northern river bank, and the LGX site (29.00° N, 93.33° E; 3127 to 3139 m a.s.l.) is located opposite to the ZXT site, on the southern river bank (Fig. 1). We collected 79 cores from 41 cypresses of both living and dead trees at the ZXT site and 35 cores from 20 living trees at the LGX site. In total, 114 increment cores from 61 trees were extracted with an increment borer at breast height for the composite Langxian (LXA) chronology (Table 1).

2.3. Chronology development

All the cores were air-dried and mounted on grooved sticks with the transverse surfaces facing upward (Phipps 1985). Cores were prepared with razor blades to expose ring details to the cellular level (Stokes & Smiley 1968). Ring widths were registered with a LINTAB 6 measuring system with a resolution of 0.01 mm, and all series were cross-dated by visual inspection (Stokes & Smiley 1968) and by statistical tests (sign tests and *t*-tests) using the software package TSAP-Win (Rinn 2003). Before establishing the chronology, the COFECHA (Holmes 1983) program was applied to check the cross-dating quality for the Langxian samples. To avoid reduction of sample depth and in order to develop a long chronology, we included all the samples for analysis. The LXA chronology was ultimately produced from the ZXT and LGX sites (the mean correlation coefficient was 0.396 among all the dated Langxian series). To develop a regional chronology, we included 197 ring-width series from the previous studies from south-central Tibet, i.e. 140 series from the Sangri chronology (SR), and 57 series from the Langkazi chronology (LKZ) (Liu et al. 2010b, 2011). The regional combined series was denoted as the SLLreg chronology (Table 1).

Table 1. Tree-ring sites and their locations. ZXT and LGX are sampling sites from Langxian county; their combined series is named LXA. SRBB and SRQK are sampling sites from Sangri county; their combined series is named SR (Liu et al. 2011). LKZ is the sampling site from Langkazi county (Liu et al. 2010b). SLLreg is the regional combined series of LXA, SR and LKZ for the southern Tibetan Plateau

Site	County	Latitude (°N)	Longitude (°E)	Elevation (m a.s.l.)	Core/Tree no.	Length (yr)	Period
ZXT	Langxian	28.90	93.30	3080–3420	79/41	1066	945–2010
LGX		29.00	93.33	3127–3139	35/20	930	1181–2010
LXA (combined)		28.90–29.00	93.30–93.33	3080–3420	114/610	1066	945–2010
SRBB	Sangri	29.38	91.03	4275–4420	47/24	495	1514–2008
SRQK		29.30	91.97	4434–4550	93/48	770	1239–2008
SR (combined)		29.3–29.4	91.97–92.03	4275–4550	140/720	770	1239–2008
LKZ	Langkazi	28.97	90.43	4460–4678	57/30	442	1567–2008
SLLreg (combined)	Regional	28.90–29.3	90.43–93.33	3080–4678	311/163	1066	945–2010

The LXA and the SLLreg ring-width chronologies were developed using the program ARSTAN (Cook 1985). Prior to standardization, a data-adaptive power transformation was applied to remove bias caused by heteroscedasticity (Cook & Peters 1997). Ninety-five percent of the whole series (293 sub-series) was conservatively detrended, either by fitting a negative exponential function or a linear regression function of any slope to remove the biological age inherent in the raw data series. Because of a poor match of the conservative growth changes in the detrending function, 5% of the whole series (18 sub-series) was detrended by cubic spline with a 50% frequency-response cut-off equal to 67% of the series length.

The final tree-ring chronology was obtained by calculating residuals or differences between the transformed ring-width measurements and the fitted splines. All detrended series were averaged to chronologies by computing the biweight robust mean (Cook & Kairiukstis 1990). Variance stabilization (Osborn et al. 1997) was applied to adjust for changes in variance associated with declining sample size over time. Because the sample size declined in the early portion of the tree-ring chronology, a level of 0.85 in the expressed population signal (EPS; Wigley et al. 1984) and the mean inter-series correlations (Rbar) were calculated using a 30 yr moving window with 15 yr overlaps to determine the reliable time span. A common-period analysis from 1500 to 2000 was conducted for the standard chronology. Several commonly used descriptive statistics were also computed for the LXA and SLLreg chronologies. The mean sensitivity evaluates the climatic signal strength of the site chronology, and the first-order autocorrelation (AC1) expresses the influence of the previous year of the tree growth on the current year (Table 1).

2.4. Climate data

The closest meteorological station, Jiacha (29.15° N, 92.35° E; 3260 m a.s.l.), was not selected for the calibration of the tree-ring–climate relationships because of its short time span of records (only 18 yr recorded since 1991). We chose the Linzhi, Longzi,

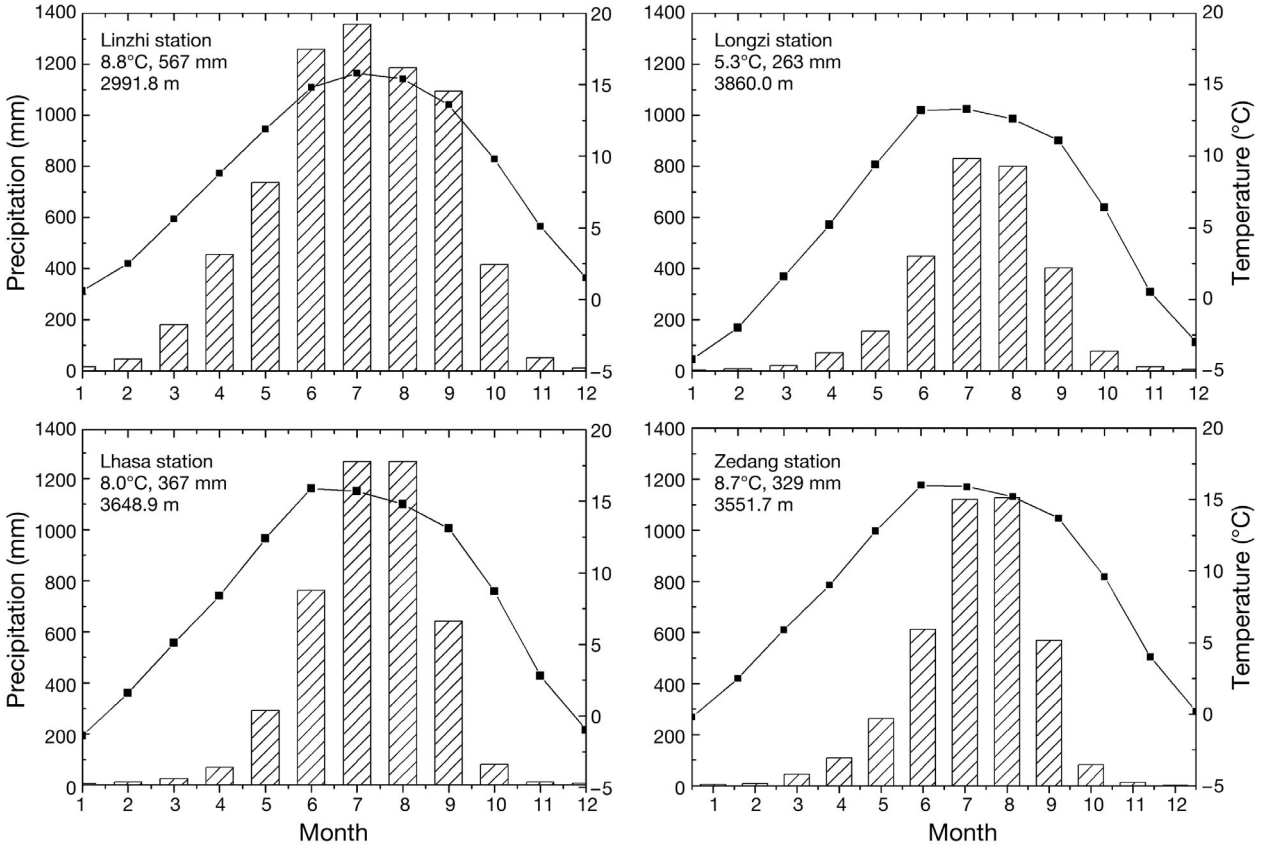

Fig. 2. Climate diagrams for meteorological stations for the period 1960–2009. Lines indicate monthly temperature, and bars indicate monthly precipitation

Lhasa, and Zedang stations in the nearby region because they are affected by the same climate regime (Figs. 1 & 2). Table 2 gives details of the instrumental data sets for the common period 1960–2009. To investigate the regional climatic variation, we merged the monthly climatic variables using the regional time series calculating method by Jones & Hulme (1996), and the calculated monthly temperature and precipitation time series were identified as REG_T and REG_P. We used the nearest monthly PDSI (Palmer 1965) data with global coverage based on a 2.5° × 2.5° grid (Dai et al. 2004), which had a span of 1960–2004, to investigate the incorporating effect of temperature, precipitation, and soil moisture on tree growth. We also extracted monthly precipitation data from high-resolution climate data points from Climate Research Unit CRUts2.1 (0.5° × 0.5° grid; Mitchell & Jones 2005). The available period of CRUts2.1 data starts from 1901, but we only used the time span of 1960–2002 because there were no instrumental observations in this region prior to 1960. Mean values were calculated from the average of 4 grid boxes, covering the region 28.75 to 29.25° N and 92.75 to 93.25° E.

To demonstrate the spatial representation, correlation analyses were conducted using the KNMI climate explorer (Royal Netherlands Meteorological Institute; http://climexp.knmi.nl) with the CRUts3.0 monthly mean field of high resolution (0.5° × 0.5° grid; Table 2).

We conducted correlation analyses (Fritts 1976) between the regional chronology SLLreg and climate data from individual stations and regional averaged series (REG_T and REG_P) over the common period (1961–2009), using the software DendroClim 2002 (Biondi & Waikul 2004). Gridded instrumental data (PDSI and CRU precipitation) were also analyzed.

3. RESULTS AND DISCUSSION

3.1. Statistical characteristics for the Langxian samples

Table 3 shows the results of dating quality checked by the COFECHA program for the Langxian samples of raw data. The master chronology covered the period from A.D. 945 to 2010, with a mean segment length of 332 yr. The mean correlation coefficient between individual series and the master chronology was 0.52 ($p < 0.01$), indicating high coherency among all the Langxian series. The mean sensitivity was at a level of 0.38, indicating that the new data set contained enough climate signals.

The LXA chronology was produced by combining specimens from the ZXT and LGX sites. Trees at the LGX site were sampled at approximately 3100 m, and samples at the ZXT site were collected at elevations ranging from 3080 to 3420 m. Although the elevation difference was large within the ZXT site, there is no obvious discrepancy between the chronologies developed from high and low elevations.

Table 2. Instrumental data sets. Lin, Log, Lha, and Zed are Linzhi, Longzi, Lhasa, and Zedang stations, respectively; CRU: four gridded monthly precipitation data of CRUts2.1 from Mitchell & Jones (2005) (0.5° × 0.5°; the original data can be downloaded from www.cru.uea.ac.uk/cru/data/hrg/); PDSI: the closest Palmer drought severity index grid (Dai et al. 2004); REG: regionally weighted temperature and/or precipitation series averaged from the Longzi, Lhasa, and Zedang stations. M: data collected from meteorological stations; G: gridded climate records; C: combined data

	Type	Latitude (°N)	Longitude (°E)	Elevation (m a.s.l.)	Length (yr)	Period
Lin	M	29.40	94.20	2991.8	56	1954–2009
Log	M	28.28	92.28	3860.0	51	1959–2009
Lha	M	29.40	91.08	3648.9	55	1955–2009
Zed	M	29.15	91.46	3551.7	54	1956–2009
CRU	G	28.75–29.25	92.75–93.25	4317–4663	43	1960–2002
PDSI	G	28.75	93.25		46	1960–2005
REG	C	28.28–29.40	91.08-94.20	2991.8–3860.0	49	1961–2009

Table 3. Statistical characteristics for raw measurement of LXA samples. r: mean correlation coefficient with master series; 'Mean measurement' describes ring width. AC1: first-order autocorrelation

	Period	Length (yr)	Mean segment length (yr)	Core/Tree no.	r	Mean measurement (mm)	SD	Mean sensitivity	AC1
LXA	945–2010	1066	332	114/61	0.52	0.80	0.52	0.38	0.73

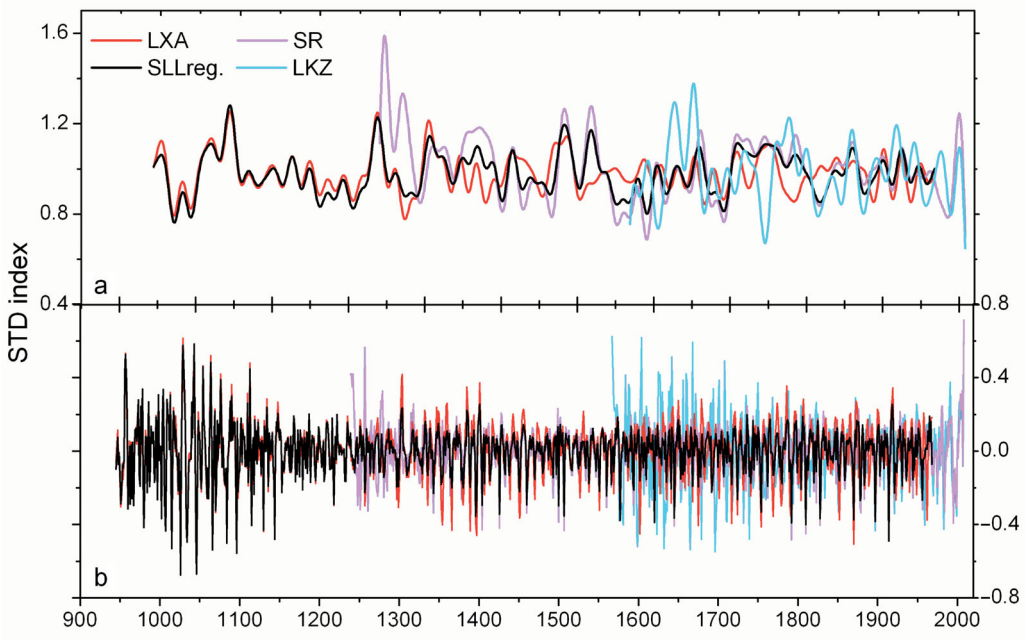

Fig. 3. (a) Visual comparison for the 20-yr low-pass filtered LKZ, SR, LXA, and SLLreg series. (b) 20-yr high-pass bands for the same series. STD: standard chonology. Abbreviations in Table 1

3.2. Statistical characteristics of the LXA and SLLreg standard chronologies

The correlations between the LKZ, SR, and LXA chronologies and their regional combined SLLreg chronology were 0.26, 0.93, and 0.64, respectively, over their common 1567–2008 period, with small differences being obtained from their 20 yr low-pass (0.21, 0.96, and 0.71) and high-pass fractions (0.21, 0.91, and 0.71) (Fig. 3). The significant correlations suggest that it is reasonable to combine tree ring-width series from 3 single sites to develop a composite chronology. Moreover, the LXA chronology correlated with the regional combined SLLreg chronology at 0.66 over their common 1300–2010 period, with higher correlation coefficients in their 20-yr low-pass ($r = 0.98$, $p < 0.01$) and high-pass fractions ($r = 0.79$, $p < 0.01$). The good correlations implied that the new LXA tree-ring data enhanced the regional chronology. The long-term time span of the LXA chronology provided the foundation to analyze the regional climatic variations in the southern TP.

Standard chronologies and their sample depths for the LXA and SLLreg were demonstrated over their whole time span from 945 to 2010 (Fig. 4). The Rbar values for both the LXA and SLLreg chronologies tended to increase before A.D. 1200, which results from the decrease of sample depth around A.D. 1200. However, the Rbar values were above 0.2 over most of the last millennium for both chronologies, indicating statistical fidelity. The most confident time span was A.D. 1300–2010 for the regional SLLreg chronology based on the EPS threshold value of 0.85. Descriptive statistical characteristics of the SLLreg chronology showed that cypress in this region was a favorable species for dendroclimatological analysis (Table 4). To sum up, all the statistical values indicated that radial growth in this region responded to climatic forcing.

3.3. Regional climate variability

Comparing the monthly mean temperature and precipitation data from the 4 meteorological stations, the climate variability during the past 49 yr rendered similar variations. The annual mean temperatures were 8.8, 5.3, 8.0, and 8.7°C, and the annual precipitation values were 567, 263, 367 and 329 mm, for the Linzhi, Longzi, Lhasa, and Zedang stations, respectively (Fig. 2). A noticeable difference between Linzhi and the other stations occurred when mean annual temperature and precipitation at Linzhi were at their highest. To account for these differences in the instrumental records, a 10 yr low-pass filtering was applied to the temperature/precipitation records (Fig. 5). The 4 records showed similar behavior for both temperature and precipitation visually, with higher agreement in the low-frequency domain. A distinctive difference in precipitation at Linzhi occurred during the 1980s and the 1990s; this was high in comparison to long-term precipitation trends in the records of the other 3 stations, partly because of its distance from the other stations and its different topography (Liu et al. 2002). Different trends among

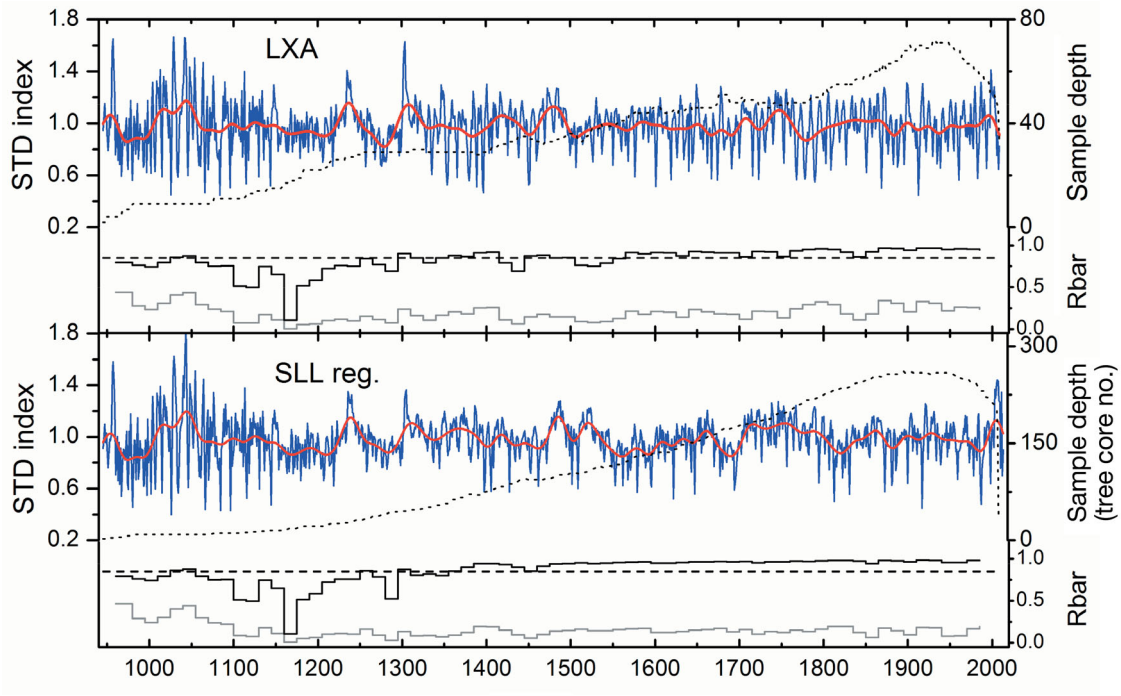

Fig. 4. STD chronology (blue), sample depth (black dotted line), running mean inter-series correlations (Rbar; grey) and expressed population signal (EPS; black) for the LXA and SLLreg series. The black dashed line denotes the EPS 0.85 criterion; the red bold line indicates 11-yr fast Fourier transform smoothing

the various meteorological records made the statistical differentiation and selection of the most appropriate instrumental data exceptionally challenging. As a result, we chose only Longzi, Lhasa, and Zedang station records to calculate the regional climate series. The regional mean temperature (REG_T) was 7.04°C and a warming trend in the southern TP during the late 20th century was prominent. The regional mean precipitation (REG_P) showed complex variation trends before 1985 and an increasing trend since then.

3.4. Growth–climate relationship

For temperature, significant positive correlations ($p < 0.05$) were found in previous Novembers at Longzi, Lhasa and Zedang (r values of 0.35, 0.42 and 0.40, respectively), as well as for REG_T (r = 0.42) (Fig. 6). The significant correlations in the non-growing season suggest that carbon fixation in winter could provide evergreen trees with accumulated cryoprotective sugars and added energy for the growing season (Schaberg 2000). The influence of temperature during seasons preceding tree growth was a common feature in the high-altitude tree-ring series, and it was reasonable to conclude that mild winters provided sufficient heat for significant tree growth in the following growth season (Bräuning & Mantwill 2004). For precipitation, a striking feature was that the correlation coefficients were positive and consistent across most months, with significant positive correlations ($p < 0.05$) found in previous and current growing seasons at the 3 stations (current March and April at Longzi station, previous June and August and current May at Lhasa station, previous July and August and current April and May at Zedang station, and previous August and current April, May, and August for the REG_P series). This distinctive characteristic was understandable due to the fact that precipitation during these months provides moisture availability in this semi-arid region and favors formation of early wood cells, which account for the majority of the total ring width.

The closest 4-box averaged CRU precipitation grids were also calculated. The results revealed negative

Table 4. Statistical characteristics for the LXA and SLLreg chronologies. R: mean correlation coefficient among series; EPS: expressed population signal; AC1: first-order autocorrelation

	R	Mean sensitivity	EPS	AC1
LXA	0.518	0.16	0.79	0.52
SLLreg	0.488	0.14	0.95	0.49

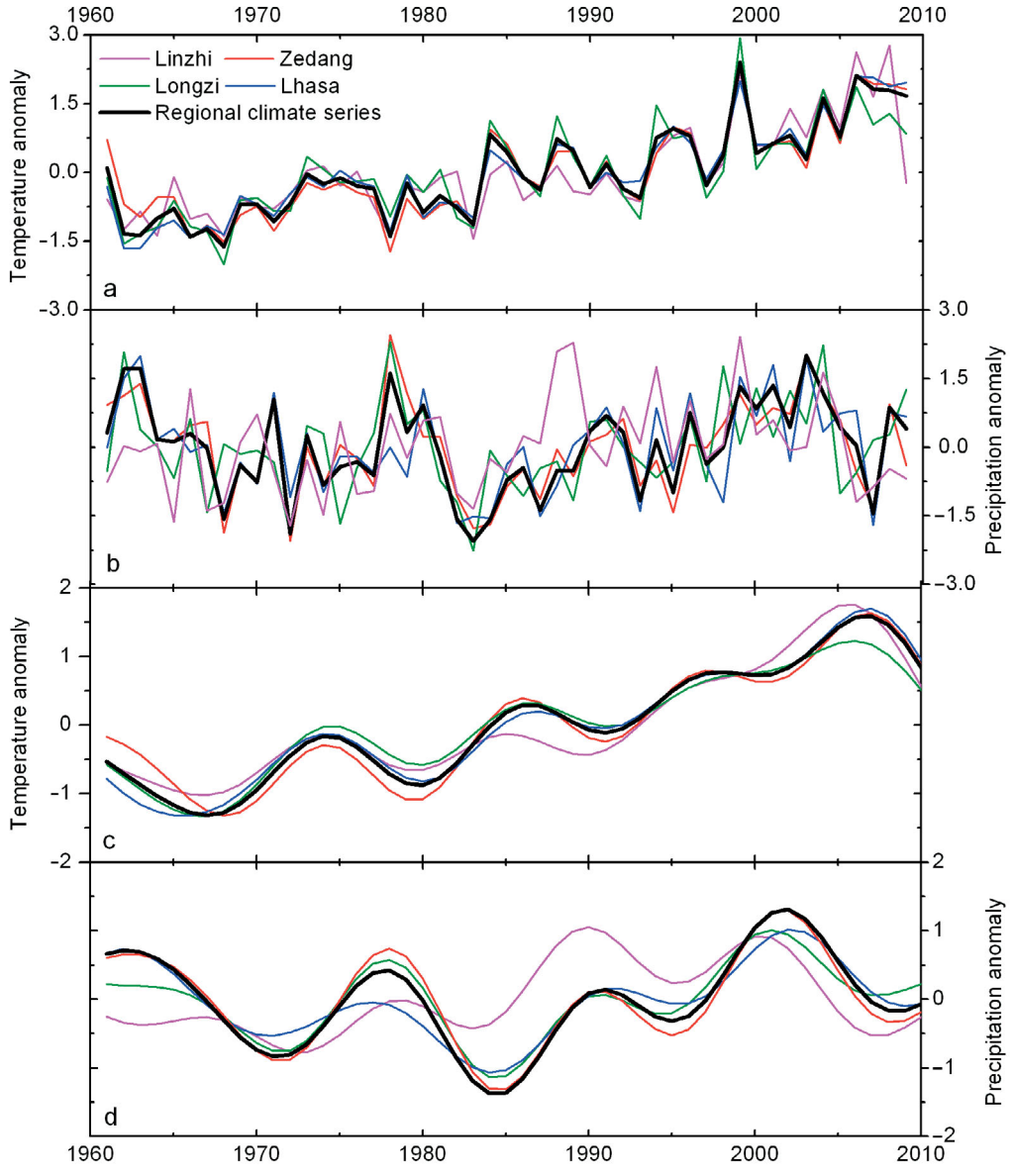

Fig. 5. (a) Unfiltered temporal changes in regional annual temperature (July–June) for the Linzhi (magenta), Longzi (green), Lhasa (blue) and Zedang (red) stations, and regional mean temperature and precipitation (REG_T and REG_P; bold black) in common periods from 1960 to 2009. (b) Unfiltered temporal changes in regional annual precipitation. (c,d) 10-yr low-pass filtered temperature and precipitation comparisons

correlation in the previous April and positive correlation in the previous May as well as in the previous and current August. Here it was noteworthy that no significant correlation was found with monthly PDSI data extracted from the closest grids. As mentioned above, the SLLreg chronology represented integrated ring-width variation in the southern TP, which was regarded as a reflection of moisture-sensitive proxy data. The results of the growth/climate relationship analysis confirmed the evidence.

Besides monthly climatic variables, we investigated the correlation coefficients between ring widths and various seasonal assemblages of monthly precipitation and sub-grouped grid data sets (Fig. 7). Correlations between SLLreg and meteorological records, along with 4-box averaged CRU precipitation grids and PDSI data of the same seasonal assemblages, were found to be insignificant. The strongest correlation (0.563, $p < 0.01$) was found with annual REG_p from the previous July to the current June during the common period from 1961 to 2009. Although the most significant correlation between the SLLreg chronology and monthly precipitation was found during the warm season (June–September), the

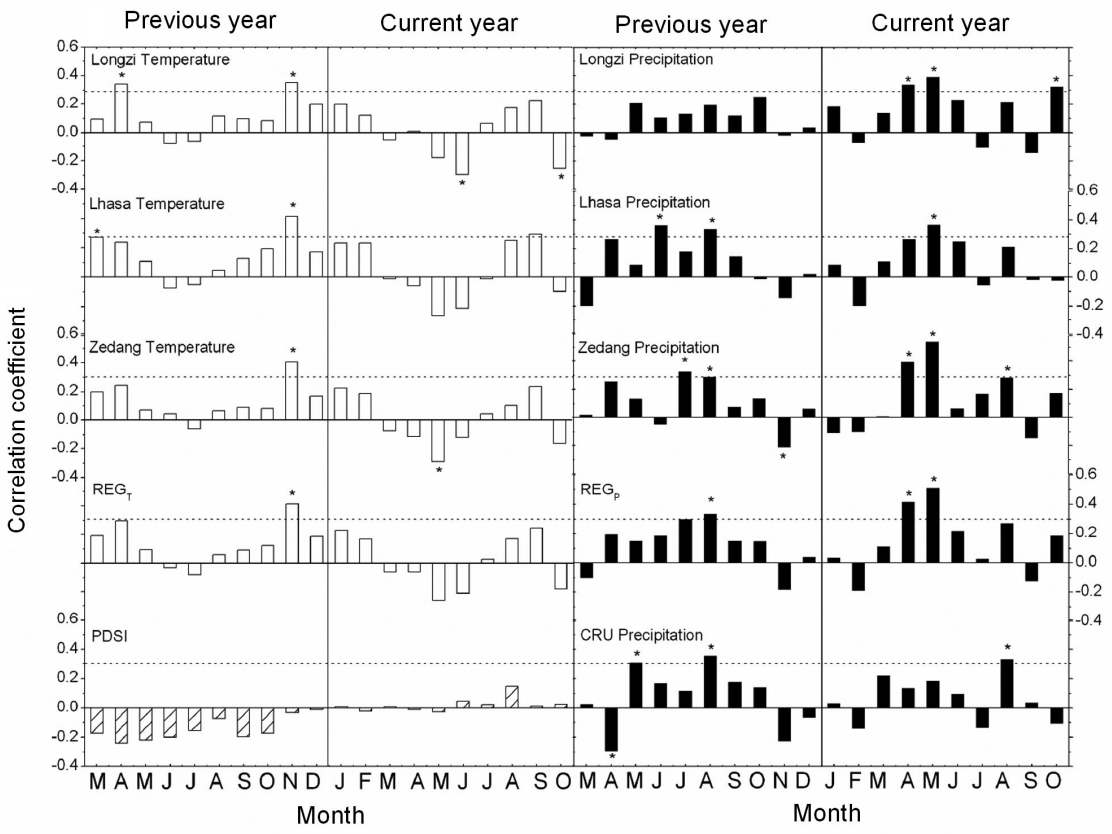

Fig. 6. Climate correlations between the SLLreg regional chronology and Longzi, Lhasa, and Zedang temperature (white—including REG_T temperature) and precipitation (black—including CRU and REG_P precipitation), as well as CRU precipitation, PDSI (shaded bars), from the previous March to the current October over 1961–2009 common periods. Horizontal dashed lines: 95 % confidence intervals. *Response functions significant at the 0.05 level

correlation coefficient was only 0.42 ($p < 0.01$). This result verified that the SLLreg chronology more closely reflected an annual rather than a warm-season climatic signal.

To emphasize the climate significance of the new data set, we compared the LXA ring-width index and the monthly precipitation at the Jiacha station (the closest meteorological station to the LXA sampling sites) during the common period from 1992 to 2010. The correlation coefficient between LXA chronology and Jiacha precipitation (July–June) was 0.79 ($p < 0.01$), indicating that the Langxian tree growth responds to annual precipitation. However, the shorter time span of instrumental records (<19 yr) at Jiacha station was not strong enough for the calibration to reconstruct the local precipitation variability using the LXA chronology.

It was useful to test whether the correlations for the regional chronology and the instrumental records were consistent across all months at the closest meteorological station. The tree growth/climate analysis between SLLreg and monthly precipitation at Jiacha station was conducted from the prior March to the current October for the available common period 1992–2010 (data not shown). The results displayed correlation patterns similar to those between SLLreg and monthly REG_P series (Fig. 6). The correlation coefficient for annual (July–June) precipitation at Jiacha station with SLLreg chronology was 0.65 ($p < 0.01$), implying that annual precipitation was the controlling factor for tree growth at the study region.

3.5. Annual precipitation reconstruction and its temporal variations

The SLLreg chronology extracted from the southern TP was sensitive to the regional annual (July–June) precipitation. We calibrated the SLLreg chronology against annual (July–June) precipitation values from the REG_P series (Fig. 8). The high- and low-frequency relationships are shown in Fig. 8a and Fig. 8b, respectively. The correlations demonstrated that the amount of unexplained ring-width/instrumental data variability was mainly restricted to the high-frequency domain. For the 2 unfiltered series (Fig. 8c),

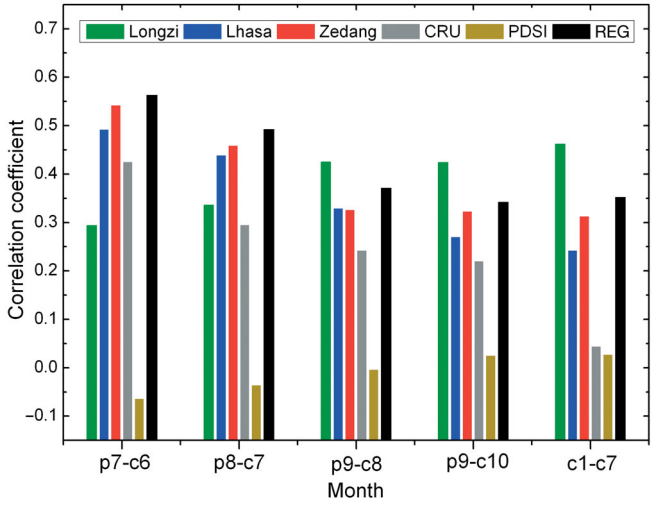

Fig. 7. Comparison of different seasonal assemblages of correlations between ring width and precipitation at the Longzi, Lhasa, and Zedang stations, as well as CRU precipitation, PDSI and REG_p. The seasonal assemblages comprise the previous July to the current June (p7–c6; p: previous; c: current), the previous August to the current July (p8–c7), the previous September to the current October (p10–c9), and the current growth season from January to July (c1–c7)

the chronology correlated at 0.64 with the precipitation data during the 1985–2009 calibration period and at 0.48 over the 1961–1984 verification period. The correlation was 0.563 for the calibration period 1961–2009, which accounts for 31.73% of instrumental precipitation data. Regression of the proxy data against instrumental precipitation data over the 1961–2009 calibration period was 0.27 (leave-one-out value; Michaelsen 1987), indicating some useful information in the regression reconstruction (Cook et al. 1994), although there was no significance test for other verification parameters, such as the sign test, reduction of error, product means, etc.

We also carried out multiple linear regression using the chronologies of the current year (t) and following year (t+1). The regression model was $Y = 145.199 + 132.649X_t + 0.074X_{t+1}$, where Y is the July–June precipitation, and X_t and X_{t+1} are tree growth for the current year and the following year, respectively. The correlation coefficient was 0.57 ($p < 0.01$, $F = 10.81$). In comparison, the correlation coefficient for the SLLreg/REG_p comparison was 0.563 ($p < 0.01$). The multiple regression model was not good as expected, and therefore it was inappropriate to adopt the regression model for reconstruction.

To capture the full range of natural precipitation variability, we employed scaling instead of the regression method. The procedure was manipulated by scaling the SLLreg chronology to the meteorological data REG_p for their common period (1961–2009), i.e. the variance and mean of the proxy record were set equal to those of the instrumental data (Esper et al. 2005). The low-frequency relationship between the ring-width and the meteorological data REG_p was much stronger after dividing the two into 7 yr high-pass ($r = 0.28$, $p < 0.01$) and low-pass ($r = 0.77$, $p < 0.01$) components (Fig. 8a,b). These correlations demonstrated that the amount of unexplained ring-width and instrumental data variability was mainly restricted to the high-frequency domain. Correlations between the actual and estimated annual precipitation values were significant ($p < 0.01$) from 1985 to the present. Correlations between actual and estimated 7 yr high-pass components were, however, consistently significant during the calibration period ($r = 0.34$, $p < 0.01$; Fig. 8a). Because the estimated precipitation signal was stronger at lower frequencies (>7 yr) than at higher frequencies (<7 yr), our ring-width chronology represented precipitation variations at the low-frequency domain.

There are several potential sources of uncertainty for the SLLreg record. Samples from the ZXT site became exceptionally scarce in the 12th century, causing insufficient chronology replication around the 1150s. Limited availability of instrumental station data that reflected climate conditions of the high-elevation sampling sites hindered our ability to calculate the growth/climate relationship over longer intervals. Because the closest Jiacha station failed to record a longer span of data sets, we adopted the weighted regional instrumental series for calibration, which possibly blurred the elevation differences in the study region. Previous studies have also documented that the explained variance will increase by >50% if the distance is <6 km from the meteorological stations (e.g. Liu et al. 2002).

Low-frequency variations for precipitation in southern Tibet were elucidated by applying an 11-point fast Fourier transform (Fig. 8d). During the past 666 yr, relatively wet years with above-average precipitation occurred in 1342–1391, 1383–1387, 1408–1423, 1453–1458, 1473–1492, 1508–1524, 1657–1667, 1701–1731, 1742–1768, 1781–1788, 1854–1868, 1917–1933, and 1994–2006, whereas relatively dry years with below-average precipitation prevailed during 1388–1407, 1424–1452, 1459–1472, 1493–1507, 1525–1656, 1668–1700, 1732–1741, 1769–1780, 1789–1853, 1869–1916, and 1934–1993. The 1700s–1800s was the most extended wet interval, whereas the 1550s–1650s appeared to be the most prolonged dry stage. A striking feature was that the last 2 decades (1980s–

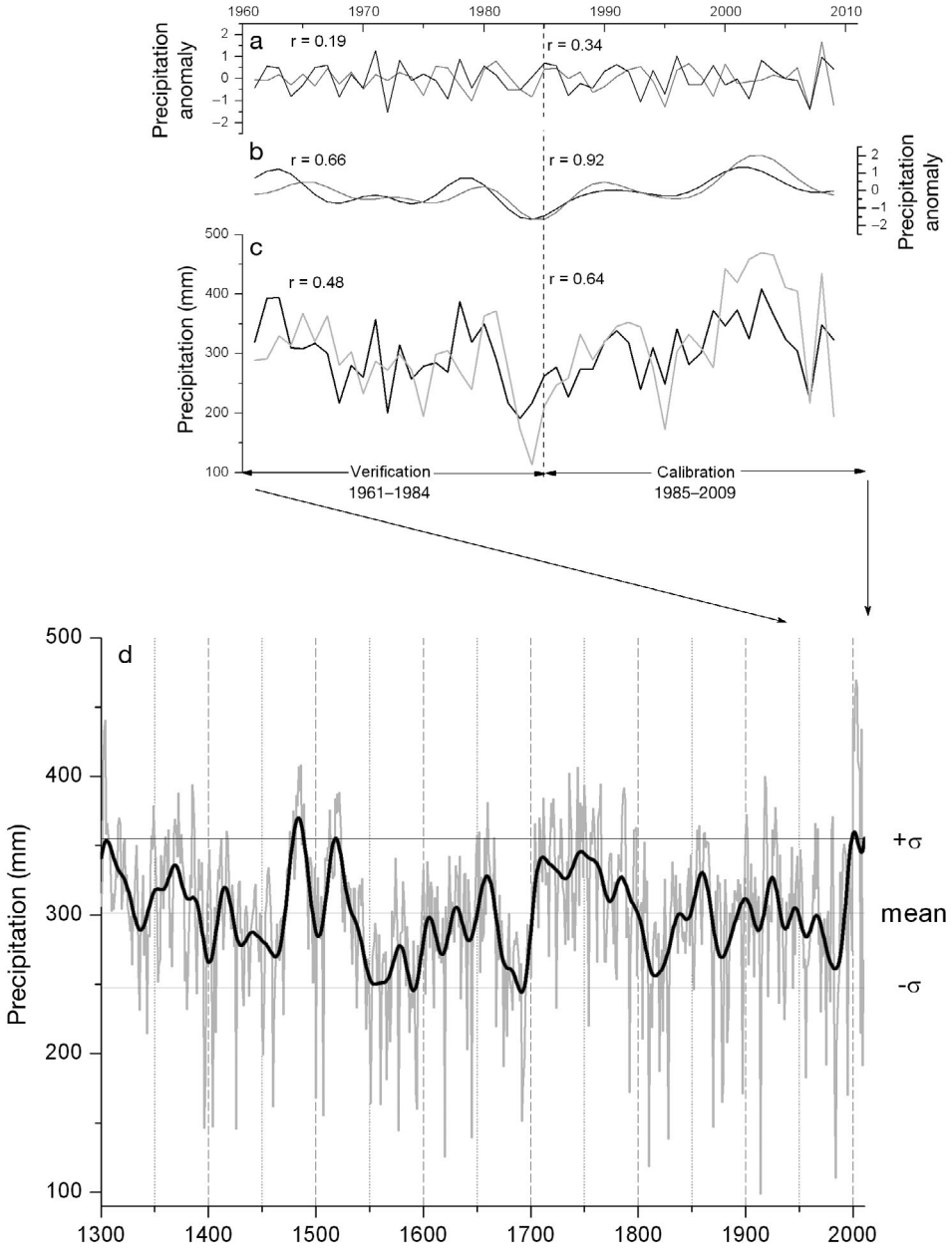

Fig. 8. (a) Comparison between 7-yr high-pass filtered July–June precipitations of REG_P (black) and simple-scaling estimated precipitation (grey) for the common period 1961–2009. (b) As for A, but 7-yr low-pass filtered. (c) Visual comparison between observed (black) and estimated (grey) precipitation. (d) Scaling-based annual (July–June) precipitation reconstruction (grey line) and its 11-yr fast fourier transform smoothing (black) for the southern Tibetan Plateau during 1300–2010. Horizontal line: long-term mean; horizontal dotted lines: ±SD

2000s) witnessed unprecedented pluvial conditions from the perspective of the past 6 centuries. The remarkable dry interval from 1530 to 1703 during the Little Ice Age corresponded to low summer temperatures around 1700 in eastern Tibet (Bräuning & Mantwill 2004).

Common wet periods in the 1510s–1540s and 1750s–1800s, and the dry periods in the 1550s–1600s, 1850s, 1920s, and 1980s were investigated with other moisture-related reconstructions based on tree rings in northeastern Tibet (Wang et al. 2008) and the southeastern TP (Fang et al. 2010). Fan et al. (2008) reconstructed moisture-related (PDSI) series derived from a ring-width chronology in the Hengduan Mountains of the southeastern TP. The first principal component of the composite chronology accounted for 60.5% of the total variance over the past 5 centuries during the common period (1655–2005) of the

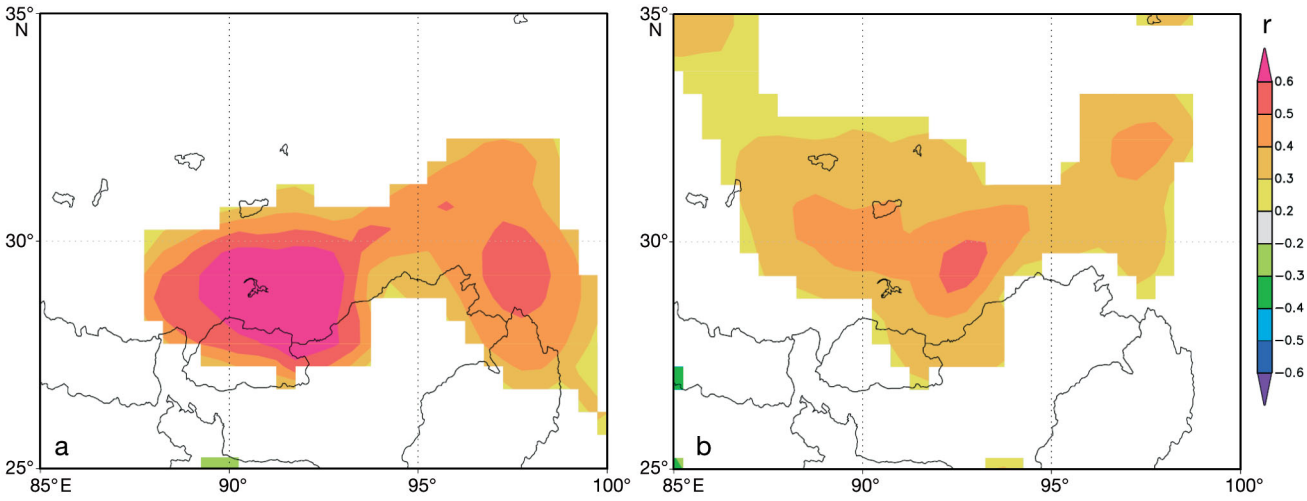

Fig. 9. Spatial correlations of (a) instrumental and (b) reconstructed annual (July–June) precipitation with regional gridded July–June precipitations for the period 1961–2005. The analyses were performed using the KNMI Climate Explorer (Royal Netherlands Meteorological; http://climexp.knmi.nl). The gridded climate data set was developed by the Climatic Research Unit (CRUts3.0)

4 single-site chronologies. The final reconstruction captured 42% of the actual PDSI variations during the common calibration period (1951–2000). Despite seasonal differences in the various precipitation reconstructions, the extended wet periods around the 1470s–1500s, 1700s–1730s, and 1770s–1800s, and the dry periods during the 1530s–1580s and the 1960s–1990s noted in our reconstructions were contemporaneous with Fan et al.'s (2008) on the southeastern TP.

To demonstrate that our reconstruction and instrumental records reflected regional-scale precipitation variability, we correlated these data with the 0.5° × 0.5° CRUts3.0 data set of all grid cells available for a user-defined region. The analyses were achieved using the KNMI Climate Explorer (Royal Netherlands Meteorological Institute; http://climexp.knmi.nl) (Fig. 9). Instrumentally recorded annual regional precipitations (REG_p) in our study area, as well as reconstructed July–June precipitations, correlated significantly with gridded precipitations on a regional scale. Spatial correlation fields were similar for the instrumental and reconstructed precipitation variability, although correlations were lower for the latter. The highest correlation fields were confined to our study regions. These results indicated that our annual precipitation reconstruction captures climatic variations for a large spatial representation in the southern TP.

Cook et al. (2010) made good first steps in the study of regional moisture variation using tree-ring chronologies from 327 sites in Asian monsoonal area to reconstruct the gridded PDSI for the past 700 yr. Although the reconstructed seasonal PDSI covered 534 grid points, limited PDSI grid points were reconstructed in the southern TP, where their tree-ring network merely distributed along the marginal Himalayas and the Hengduan Mountains. Because of the lack of a long tree-ring chronology in the interior southern TP, their PDSI reconstruction was derived from the weighted ensemble of nearby tree-ring sites (a series of ring-width data collected from the eastern TP and the Hengduan Mountains in the southeastern TP) through expanded search radii (more than 500 km) as described in the 'point-by-point regression' method (Cook et al. 2007). As a result, the foundation of the PDSI reconstruction may rely on teleconnections between the tree-ring chronology and the 'target' PDSI point during the defined calibration period (1951–1989).

Nevertheless, we compared our regional precipitation reconstruction for southern Tibet (SRP) with the gridded PDSI reconstructions by Cook et al. (2010). For comparison, the 2 closest reconstructed PDSI points (31.25° N, 91.25° E; 31.25° N, 93.75° E) from the central-southern TP (STP) and 5 points (26.25 to 28.75° N, 96.25 to 101.25° E) from the Hengduan Mountains on the southeastern TP were extracted. An averaged PDSI time series was calculated from the former 2 points on the STP, and another averaged PDSI series was computed from the latter 5 points in the Hengduan Mountains (HDP).

In order to discuss whether the climate variability for the southern TP was different from or similar to that for the northern TP over the past 7 centuries, we selected tree-ring series derived from the northern TP for comparison. Yang et al. (2010a) analyzed spa-

tial and temporal growth variations of Qilian junipers over the northeastern TP during the period 1450–2001 by applying the empirical orthogonal function (EOF) technique to 7 moisture-sensitive ring-width chronologies. The first principal component (PC1) accounted for 51.58% of the total variance and was regarded as an indicator of regional precipitation variations in the northern TP. To better elucidate the spatial patterns of the moisture variations in the southern and northern TP over the past 700 yr, we normalized all the reconstructions of moisture change for visual inspection of periods of above- and below-average values. Including our annual precipitation reconstruction for southern TP (SRP), the 4 tree-ring-based reconstructions (SRP, PC1, STP, and HDP series) were all smoothed with a 20-yr low-pass filter approach to highlight the low-frequency climate signals (Fig. 10).

According to Fig. 10, the SRP displays patterns of wet/dry variations consistent with the gridded PDSI reconstruction of the STP by Cook et al. (2010). The in-phase variation registered by the STP and HDP reconstructions agreed well with our precipitation reconstruction (Table 5). Additionally, wet/dry phases recorded in the HDP reconstruction were in phase with the spring (March–May) drought reconstruction

Table 5. Correlations for the SRP, STP, and HDP series during their common wet/dry intervals. All correlation coefficients were significant at 99%

	Common period	r
SRP vs. STP	1300–2000 (whole period)	0.30
	1300s–1390s	0.54
	1500s–1530s	0.62
	1710s–1780s	0.18
	1870s–1960s	0.36
SRP vs. HDP	1300–2000 (whole period)	0.13
	1310s–1370s	0.25
	1510s–1550s	0.83
	1880s–1930s	0.45

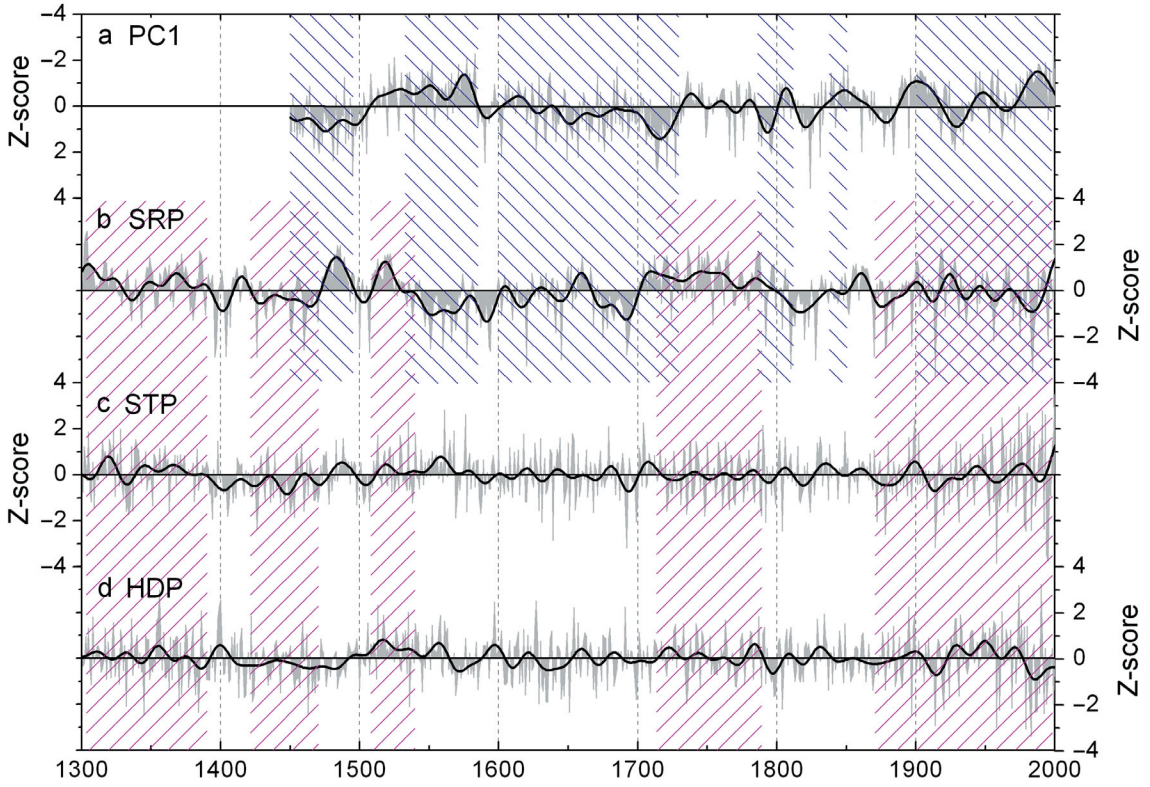

Fig. 10. Comparison of various moisture reconstructions for the Tibetan Plateau derived from tree-ring records. (a) PC1 of 7 moisture-sensitive ring-width chronologies over the Qilian Mountains (Yang et al. 2010a); (b) annual (July–June) regional precipitation reconstruction for the south Tibet (SRP; present study); (c) summer (June–July–August) drought reconstruction extracted from 2 averaged PDSI points (31.25° N, 91.25° E; 31.25° N, 93.75° E) in the southern TP (STP; Cook et al. 2010); (d) summer (June–August) drought reconstruction extracted from 5 averaged PDSI points (26.25–28.75° N, 96.25–101.25° E) in the Hengduan Mountains, southeastern TP (HDP; Cook et al. 2010). All series were adjusted for their long-term means over the common period 1300/1450–2000, and smoothed with a 20 yr low-pass filter (bold line) to emphasize long-term fluctuations. Blue hatching: contrasting wet/dry moisture variations between the northern and southern TP during the past 550 yr. Magenta hatching: contemporary moisture variations in the southern TP during the past 700 yr

in the Hengduan Mountains by Fan et al. (2008). This correspondence implies that both reconstructions are robust. Similar variations recorded by our reconstruction and Cook et al.'s, along with Fan et al.'s, reflected common regional climatic variation pattern over the southern TP during the past 7 centuries.

It was noteworthy that the dry (wet) spells registered by the PC1 in the northern TP corresponded with high (low) precipitation periods recorded by the SRP in the southern TP during most of the past 550 years. Typical periods were during the 1450s–1495, 1530s–1585, 1600s–1720s, 1785–1814, 1935–1850, and 1900–2000 periods. For the longest of these periods—1600s–1720s and 1900–2000—the SRP and PC1 series correlated at 0.49 and 0.53, respectively ($p < 0.01$; the PC1 series was inverted for better visual comparison). Those typical intervals and significant correlations might imply non-stationary opposite relationships of moisture variation over the past 5 centuries for the northern or southern TP.

Lin & Zhao (1996) performed oblique rotated principal component analysis of the monthly mean precipitations collected from 50 meteorological stations in the TP, and demonstrated that the change of precipitation had a contrary variation trend between the north and the south. By comparing precipitation accumulation derived from ice cores, Duan et al. (2008) suggested that precipitation in the northern TP varied out of phase and contrastively to the southern TP during the past 700 yr. A recent analysis on stable isotopes of the precipitation on the TP showed that the southern part of the TP, divided by the southwest Tanggula Mountains, was mainly under the influence of the SASM, and the moisture was directly from evaporation from the Indian Ocean (Tian et al. 2006); the northern part of the TP, especially High Asia, was mainly affected by moisture evaporation from the Atlantic Ocean (Numaguti 1999). Therefore, the difference in moisture sources and the spatiotemporal variations in precipitation between the northern and southern TP can be attributed to the control of different atmospheric circulation, the SASM and the Westerlies.

Wang et al. (2005), using an NCEP/NCAR reanalysis of the gridded climate data, showed that the differences in moisture sources between the northern and southern TP were divided by the convergence shear line around 35°N latitude. This conclusion was drawn from the comparison of annual variation between the first eigenvector of atmospheric moisture transport flux divergence and the SASM index ($r = 0.42$, $p < 0.01$) as well as the correlation between the second eigenvector and the westerly index ($r = 0.75$, $p < 0.001$). The EOF analysis of the atmospheric moisture transport flux divergence revealed that the position of the convergence shear line affected the precipitation variation in the northern and southern TP. If the convergence shear line moved northward, the precipitation decreased in the northern TP because the strengthened moisture transport from the Westerlies accelerated the atmospheric moisture transport flux divergence. Meanwhile, the SASM was in a relatively strong state, and resulted in increasing precipitation in the southern TP. In contrast, if the convergence shear line retreated southward, the Westerlies would become strong and precipitation would increase in the northern TP whereas the moisture transport would weaken and precipitation decrease in the southern TP. The SASM played a major role in the Asian monsoon system and affected fluctuations in the Westerlies by adjusting the large-scale atmospheric circulation. The shift of the convergence shear line around the northern–southern TP division controlled the pendulated force between the SASM and the Westerlies, resulting in precipitation variations in the northern and southern TP.

The shift of the convergence shear line could be one of the physical processes involved in controlling the opposing patterns in moisture variation in the northern and southern TP. To further reveal the possible mechanism(s) for this seesaw phenomenon, large-scale climate systems should be incorporated into our analysis. The North Atlantic Oscillation (NAO) is one of the major atmospheric teleconnection patterns in the Northern Hemisphere (Rogers 1984) and is strongly associated with the intensity of the Westerlies (Liu & Yin 2001). The NAO influences precipitation in China through the Westerlies, which bring moist air into central Asia (including part of China). For regions that are directly influenced by the Westerlies, years when Westerlies were dominant tended to have frequent rainfall. When the Westerlies were suppressed, rainfall was reduced (Hurrell et al. 2003). Liu & Hou (1999) pointed out that the enhanced Westerlies in mid-latitudes caused by a suppressed low NAO index could induce an accompanying strengthening of the northern/southern trough over the TP by changing circulation dynamics of the Westerlies over the region.

From this point of view, we hypothesized that there might be positive relationships between the SRP and NAO index series over the past 7 centuries. Luterbacher et al. (2001) developed an NAO index series covering the period 1659–2001 based on both instrumental and documentary data. The SRP showed sim-

ilar variation with Luterbacher et al.'s series during 1660–2000, with a correlation coefficient of 0.32 ($p < 0.01$) after a 31 yr filtering. This suggests a teleconnection between the NAO and moisture variability in the southern TP. However, a weaker correlation was found for 2 periods (1660s–1710s and 1750–1780s) for the SRP and the NAO index series. We assumed that the linkage between the NAO and moisture variation pattern in the TP might be non-stationary over time.

Consequently, the mechanism for the discontinuously adverse moisture variations in the northern/southern TP over the past ~500 yr was likely linked with the interaction between large atmospheric circulations, i.e. the SASM, the Westerlies, and the NAO. However, the relationship of these large climate systems to regional climate over the past 7 centuries is still unclear. Further and more in-depth studies are required to assess the integrated performance of the SASM, the Westerlies, and the NAO, and to determine how they have affected the moisture variation modes in the northern and southern TP for the past 7 centuries.

4. CONCLUSIONS

Based on the combination of new and 2 former tree-ring data sets, we developed a regional ring-width chronology of the southern TP, spanning A.D. 945 to 2010. The regional chronology correlated at 0.563 with the regional annual (July–June) precipitation weighted from 3 nearby meteorological stations over the 1961–2009 period. The common signal (r) increased to 0.77 after 7 yr low-pass filtering. By assessing the relationship between climate and tree growth using reconstruction models, we finally chose the annual precipitation (July–June) as the best predictor and adopted the reconstruction-by-scaling method. The scaled precipitation covered the 1300–2010 period and recognized wet/dry intervals on interannual to multidecadal scales. Spatial correlation analysis with gridded land surface data revealed that our annual precipitation reconstruction contained a strong regional precipitation signal for the southern TP. Correspondence with different tree-ring-based reconstructions from the southern and southeastern TP implied that the regional precipitation reconstruction was reliable because of enough replication for the overall periods and good coherency with the gridded drought reconstructions.

Comparison with moisture-sensitive reconstructions indicated decadal to multi-decadal similarities within the southern TP. The reconstructed series also revealed a non-stationary relationship of opposite moisture variations in the northern and southern TP for the past ~500 yr. The shift of the convergence shear line was partly responsible for the discrepancy, as it controlled the intensified or weakened moisture transport brought from the SASM and the Westerlies to the TP. The comparison between our reconstructed regional precipitation and the NAO index over the past ~300 yr exhibited a non-stationary positive relationship between moisture variation in the southern TP and the NAO. One possible mechanism is linked to the fact that the NAO could induce accompanying strengthening or weakening of the northern/southern trough over the TP by changing the circulation dynamics of the Westerlies throughout the region. The integrated performance among the SASM, the Westerlies and the NAO in affecting the regional moisture variations for the past 700 yr needs further investigation, specifically through the application of an atmospheric circulation model.

Acknowledgements. The authors extend many thanks to two anonymous reviewers for their valuable comments and suggestions. This study was jointly funded by the Chinese Academy of Sciences (CAS) 100 Talents Project (no. 29082762), the National Basic Research Program of China (973 Program) (no. 2010CB950104), the National Natural Science Foundation of China (NSFC) (grant no. 40871091), and the Chinese Academy of Sciences Visiting Professorship for Senior International Scientists (grant no. 2009S1-38). The authors are also grateful to Wang Jianglin and Kang Shuyuan for their helpful suggestions.

LITERATURE CITED

Biondi F, Waikul K (2004) DENDROCLIM2002: a C++ program for statistical calibration of climate signals in tree-ring chronologies. Comput Geosci 30:303–311

Bräuning A (2001) Climate history of the Tibetan Plateau during the last 1000 years derived from a network of juniper chronologies. Dendrochronologia 19:127–137

Bräuning A, Mantwill B (2004) Summer temperature and summer monsoon history on the Tibetan Plateau during the last 400 years recorded by tree rings. Geophys Res Lett 31:L24205 doi:10.1029/2004GL020793

Cook ER (1985) A time-series analysis approach to tree-ring standardization. PhD dissertation, University of Arizona, Tucson, AZ

Cook ER, Kairiukstis A (1990) Methods of dendrochronology: applications in the environmental sciences. Kluwer Academic Press, Dordrecht

Cook ER, Peters K (1997) Calculating unbiased tree-ring indices for the study of climatic and environmental change. Holocene 7:361–370

Cook ER, Briffa KR, Jones PD (1994) Spatial regression methods in dendroclimatology: a review and comparison of two techniques. Int J Climatol 14:379–402

Cook ER, Seager R, Cane MA, Stahle DW (2007) North

American drought: reconstructions, causes, and consequences. Earth Sci Rev 81:93–134
Cook ER, Anchukaitis KJ, Buckley BM, D'Arrigo RD, Jacoby GC, Wright WE (2010) Asian monsoon failure and megadrought during the last millennium. Science 328:486–489
Dai A, Trenberth KE, Qian T (2004) A global dataset of Palmer Drought Severity Index for 1870–2002: relationship with soil moisture and effects of surface warming. J Hydrometeorol 5:1117–1130
Duan KQ, Yao TD, Wang NL, Tian LD, Xu BQ (2008) The difference in precipitation variability between the north and south Tibetan Plateaus. J Glaciol Geocryol 30: 727–732 (in Chinese)
Esper J, Frank DC, Wilson RJS, Briffa KR (2005) Effect of scaling and regression on reconstructed temperature amplitude for the past millennium. Geophys Res Lett 32: L07711 doi:10.1029/2004GL021236
Fan ZX, Bräuning A, Cao KF (2008) Tree-ring based drought reconstruction in the central Hengduan Mountains region (China) since A.D. 1655. Int J Climatol 28:1879–1887
Fang KY, Gou XH, Chen FH, Li JB and others (2010) Reconstructed droughts for the southeastern Tibetan Plateau over the past 568 years and its linkages to the Pacific and Atlantic Ocean climate variability. Clim Dyn 35:577–585
Fritts HC (1976) Tree rings and climate. Academic Press, London
Gou XH, Chen FH, Yang MX, Jacoby G, Fang KY, Tian QH, Zang Y (2008) Asymmetric variability between maximum and minimum temperatures in Northeastern Tibetan Plateau: evidence from tree rings. Sci China D Earth Sci 51:41–55
Holmes RL (1983) Computer-assisted quality control in tree-ring dating and measurement. Tree-Ring Bull 43:69–95
Huang RH, Zhang ZZ, Huang G, Ren BH (1998) Characteristics of the water vapor transport in East Asian Monsoon region and its difference from that in South Asian Monsoon region in summer. Sci Atmos Sin 22:460–469
Hurrell JW, Kushnir Y, Ottersen G, Visbeck M (2003) The North Atlantic Oscillation: climatic significance and environmental impacts. American Geophysical Union, Washington, DC
Jones PD, Hulme M (1996) Calculating regional climatic time series for temperature and precipitation: methods and illustrations. Int J Climatol 16:361–377
Li ZS, Zhang QB, Ma KP (2011) Tree-ring reconstruction of summer temperature for A.D. 1475-2003 in the central Hengduan Mountains, Northwestern Yunnan, China. Clim Change 110:455–467
Liang EY, Shao XM, Qin NS (2008) Tree-ring based summer temperature reconstruction for the source region of the Yangtze River on the Tibetan Plateau. Global Planet Change 61:313–320
Lin ZY, Zhao XY (1996) Spatial characteristics of changes in temperature and precipitation of the Qinghai-Xizang (Tibet) Plateau. Sci China D Earth Sci 39:442–448
Liu XD, Hou P (1999) Variations of summer rainfall over Qinghai-Xizang Plateau and its association with the North Atlantic Oscillation. Acta Meteorol Sin 57:561–570 (in Chinese)
Liu XD, Yin ZY (2001) Spatial and temporal variation of summer precipitation over the eastern Tibetan Plateau and the North Atlantic Oscillation. J Clim 14:2896–2909
Liu Y, Ma LM, Cai QF, An ZS, Liu WG, Gao LY (2002) Summer temperature (June-August) reconstruction in Helan Mountain since AD 1890 based on stable isotope in tree rings. Sci China D Earth Sci 32:667–674 (in Chinese)
Liu Y, Sun YJ, Song HM, Cai QF, Bao G, Li XX (2010a) Tree-ring hydrologic reconstructions for the Heihe River watershed, western China since AD 1430. Water Res 44: 2781–2792
Liu JJ, Yang B, Sonechkin D (2010b) Establishment of tree-ring chronology and climatic response of Tibetan juniper (*S. tibetica*) in south Tibet, western China. Sci Cold Arid Reg 2:493–504
Liu JJ, Yang B, Qin C (2011) Tree-ring based annual precipitation reconstruction since AD 1480 in south central Tibet. Quat Int 236:75–81
Luterbacher J, Xoplaki E, Dietrich D, Jones PD and others (2001) Extending North Atlantic Oscillation reconstructions back to 1500. Atmos Sci Lett 2:114–124
Michaelsen J (1987) Cross-validation in statistical climate forecast models. J Clim Appl Meteorol 26:1589–1600
Mitchell TD, Jones PD (2005) An improved method of constructing a database of monthly climate observations and associated high resolution grids. Int J Climatol 25: 693–712
Mohanty UC, Ramesh KJ, Pant MC (1996) Certain seasonal characteristic features of oceanic heat budget components over the Indian Seas in relation to the summer monsoon activity over India. Int J Climatol 16:243–264
Numaguti A (1999) Origin and recycling processes of precipitating water over the Eurasian continent: experiments using an atmospheric general circulation model. J Geophys Res 104:1957–1972
Osborn TJ, Briffa KR, Jones PD (1997) Adjusting variance for sample-size in tree-ring chronologies and other regional mean time series. Dendrochronologia 15:89–99
Palmer WC (1965) Meteorological drought. Weather Bureau Research Paper 45. US Department of Commerce, Washington, DC
Phipps RL (1985) Collecting, preparing, crossdating, and measuring tree increment cores. Water-Resources Investigations Report 85-4148, US Geological Survey, Denver, CO
Qin C, Yang B, Burchardt I, Hu XL, Kang XC (2010) Intensified pluvial conditions during the twentieth century in the inland Heihe River Basin in arid northwestern China over the past millennium. Global Planet Change 72: 192–200
Rinn F (2003) TSAP-Win: time series analysis and presentation for dendrochronology and related applications. Version 0.55 user reference. RimaTech, Heidelberg, available at www.rimatech.com
Rogers JC (1984) Association between the North Atlantic oscillation and the Southern Oscillation in the Northern Hemisphere. Mon Weather Rev 112:1999–2015
Schaberg PG (2000) Winter photosynthesis in red spruce (*Picea rubens* Sarg): limitations, potential benefits, and risks. Arct Antarct Alp Res 32:375–380
Shao XM, Xu Y, Yin ZY, Liang E, Zhu HF, Wang S (2010) Climatic implications of a 3585-year tree-ring chronology from the northeastern Qinghai-Tibetan Plateau. Quat Sci Rev 29:2111–2122
Sheppard PR, Tarasov PE, Graumlich LJ, Heussner KU, Wagner M, Österle H, Thompson LG (2004) Annual precipitation since 515 BC reconstructed from living and fossil juniper growth of northeastern Qinghai Province, China. Clim Dyn 23:869–881
Shi YF, Li JJ, Li BY, Yao TD and others (1999) Uplift of the Qinghai-Xizang (Tibetan) Plateau and east Asia environ-

mental change during late Cenozoic. Acta Geogr Sin 54: 10–20 (in Chinese)

Stokes MA, Smiley TL (1968) An Introduction to tree-ring dating. The University of Chicago Press, Chicago, IL

Tian LD, Yao TD, White JWC, Yu WS, Wang NL (2005) Westerly moisture transport to the middle of Himalayas revealed from the high deuterium excess. Sci China D Earth Sci 50:1026–1030

Tian LD, Yao TD, Yu WS (2006) Stable isotopes of precipitation and ice core on the Tibetan Plateau and moisture transports. Quat Sci 26:145–152 (in Chinese)

Tian QH, Gou XH, Zhang Y, Peng JF, Wang JS (2007) Tree-ring based drought reconstruction (A.D. 1855–2001) for the Qilian Mountains, northwestern China. Tree-Ring Res 63:27–36

Tian QH, Gou XH, Zhang Y, Wang YS, Fan ZX (2009) May-June mean temperature reconstruction over the past 300 years based on tree rings in the Qilian Mountains of the northeastern Tibetan Plateau. IAWA J 30:421–434

Wang KL, Jiang H, Zhao HY (2005) Atomospheric water vapor transport from westerly and monsoon over the Northwest China. Adv Water Sci 16:432–438 (in Chinese)

Wang XC, Zhang QB, Ma KP, Xiao SC (2008) A tree-ring record of 500-year dry-wet changes in northern Tibet, China. Holocene 18:579–588

Webster PJ, Magana VO, Palmer TN, Shukla J, Tomas RA, Yanai M, Yasunari T (1998) Monsoons: processes, predictability, and the prospects for prediction. J Geophys Res 103:14451–14510

Wigley T, Briffa KR, Jones PD (1984) On the average value of correlated time series, with applications in dendroclimatology and hydrometeorology. J Appl Meteorol 23: 201–213

Yang B, Qin C, Huang K, Fan ZX, Liu JJ (2010a) Spatial and temporal patterns of variations in tree growth over the northeastern Tibetan Plateau during the period AD 1450-2001. Holocene 20:1235–1245

Yang B, Kan XC, Liu JJ, Bräuning A, Qin C (2010b) Annual temperature history in Southwest Tibet during the last 400 years recorded by tree rings. Int J Climatol 30: 962–971

Yang B, Kan XC, Bräuning A, Liu J, Qin C, Liu JJ (2010c) A 622-year regional temperature history of southeast Tibet derived from tree rings. Holocene 20:181–190

Yang B, Qin C, Bräuning A, Burchardt I, Liu JJ (2011) Rainfall history for the Hexi Corridor in the arid northwest China during the past 620 years derived from tree rings. Int J Climatol 31:1166–1176

Zhang Y, Gou XH, Chen FH, Tian QH, Yang MX, Peng JF, Fang KY (2009) A 1232-year tree-ring record of climate variability in the Qilian Mountains, northwestern China. IAWA J 30:407–420

Zhang Y, Tian QH, Gou XH, Chen FH, Leavitt SW, Wang YS (2010) Annual precipitation reconstruction since AD 775 based on tree rings from the Qilian Mountains, northwestern China. Int J Climatol 31:371–381

Editorial responsibility: Nils Chr. Stenseth, Oslo, Norway

Submitted: July 18, 2011; Accepted: January 9, 2012
Proofs received from author(s): April 30, 2012